International Society for Rock Mechanics and Rock Engineering
Norwegian Group for Rock Mechanics

ISRM International Symposium
Eurock 2025 – Expanding the Underground Space
Trondheim, Norway, 16-20 June
ISBN 978-82-8208-079-8

Measuring physical aperture of a fracture affected by dislocation using photogrammetry

M. Torkan, S. Liyanarathna Vidanage, M. Aydogmus, L. Uotinen, A. Anttilainen, M. Janiszewski & M. Rinne
Department of Civil Engineering, Aalto University, Espoo, Finland
masoud.torkan@aalto.fi (email of corresponding author)

Abstract

Accurate physical aperture measurement is essential for modeling fluid flow through fractures. Stress changes, such as normal and shear stresses, can alter physical aperture, affecting flow, especially near nuclear waste sites where radionuclides may enter groundwater through fracture networks. Understanding flow under different stress conditions is key to evaluating underground excavation safety. This study focuses on accurately determining physical aperture in fractures impacted by dislocation.

A 6 cm × 6 cm × 10 cm Kuru gray granite sample with a tensile fracture was studied under dislocation. Markers with predefined distances were applied to align and scale dislocated fracture surfaces using photogrammetry. At each dislocation step, photogrammetry captured surface positions to calculate physical aperture. A local coordinate system was established for the bottom half of the sample, enabling precise measurements of the relative positions of the top and bottom surfaces with and without dislocation. The Root Mean Square Error (RMSE) of the photogrammetric measurements was approximately 35 μm. Ceramic calibration blocks were used as ground truth to assess the accuracy of the photogrammetric method. The physical aperture showed a nonlinear relationship with displacement.

This photogrammetric approach provides a deeper understanding of how dislocations change physical apertures, which can consequently affect both fluid flow behavior and shear strength. It also demonstrates the potential of photogrammetry for accurately determining physical aperture during shear tests.

Keywords

Photogrammetry, markers, accuracy, physical aperture, dislocation

1 Introduction

Rock mass serves as the foundation for many infrastructures such as dams, tunnels, and nuclear waste disposal sites, making its precise characterization crucial. Rock mass is a heterogeneous material, consisting of intact rock and discontinuities (Zhang 2005; Brady and Brown 1985). Discontinuities play a vital role in the stability and fluid flow behavior through the rock mass. Disturbances in stress conditions, due to excavations, can cause the propagation of new fractures or the opening, closing, or dislocation of existing ones. Characterizing a single rock fracture helps to better understand the fluid flow and shear behavior in fracture network and the overall stability of the rock mass (Hakami and Larsson 1996; Zimmerman and Bodvarsson 1996; Zimmerman 2005).

A single rock fracture can be influenced by both its geometrical and hydromechanical properties. These geometrical properties can, in turn, affect the hydromechanical behavior and shear strength of the fracture (National Research Council (U.S.) 1996). Geometrical properties include roughness, physical aperture, contact area, and matedness. A fracture often has two rough surfaces that may contact at certain points, known as contact points. The volume between these two surfaces is referred to as physical aperture, while surface variation is known as roughness. Matedness represents the degree of matching between the top and bottom surfaces (Chen et al. 2017; Hakami 1995; Olsson et al. 2001; Barton 1978). These parameters can change under stress; for instance, normal stress can reduce physical aperture and increase contact points, while shear stress can influence matedness and physical aperture.

To measure the geometrical properties of a fracture, both contact and non-contact methods are used. Contact methods, such as profilometry for roughness and molding or injections for measuring physical aperture, are manual, time-consuming, and often imprecise or destructive. On the other hand, non-contact methods such as laser scanning and photogrammetry can provide highly detailed, precise, and digital 3D models of fracture surfaces. Laser scanning has gained popularity because of its ease of use and the accuracy reported by manufacturers. Photogrammetry is often compared with laser scanning because laser scanning is considered a ground truth method (Yong et al. 2024). However, this comparison is not always valid because each tool should be assessed against a recognized ground truth, not merely compared to another method. For example, both photogrammetry and laser scanning results should be evaluated against a reliable benchmark or ground truth like an object with known dimensions, and the deviations between them should be examined in relation to that reference.

Numerous studies have used laser scanning and photogrammetry to estimate roughness, while research on measuring physical aperture with photogrammetry has been scarce. Physical aperture measurement for different sample sizes has been conducted with various coded marker distributions and devices such as DSLR cameras and smartphones (Torkan et al. 2022). Predefined distance coded markers were used as scale bars, where a higher number of scale bars provides more accurate results with lower Root Mean Square Error (RMSE). Photogrammetry has also been used to detect changes in physical aperture under normal stresses, with deviations ranging from 1 to 8 μm when compared to LVDTs (Torkan et al. 2024). Void geometry changes measured by pull/push tests using photogrammetry and laser scanning showed comparable accuracy (Yong et al. 2024).

The lack of knowledge and a method for measuring physical aperture affected by dislocation by photogrammetry using coded markers is the motivation for this study. The innovation of this study lies in the use of predefined coded markers as scale bars in photogrammetry to measure physical aperture affected by dislocation and the assessment of model accuracy through RMSE and ceramic calibration blocks as ground truth.

2 Methodology

2.1 Sample preparation

A 6 cm × 6 cm × 10 cm sample was extracted from a Finnish Kuru grey granite block, a homogeneous and crystalline hard rock. The block was split using the plug and feather method, which induced a tensile fracture through the block. Spaced holes were drilled along a projected crack line, and hammered plugs were used to induce the tensile fracture, after which the desired sample size was cut. Fig. 1 (a), (b), and (c) show the sample in a well-matched position, the bottom half, and the top half, respectively.

(a) (b) (c)

Fig. 1 The Kuru granite sample with dimensions of 6 cm × 6 cm × 10 cm: (a) in a well-matched position, (b) the bottom half, and (c) the top half.

2.2 Photogrammetry

2.2.1 Principle of photogrammetry

Photogrammetry is a powerful method that uses multiple photos to generate 3D models of a sample by finding matching points among overlapping images. After identifying and aligning these matching points, a sparse 3D point cloud is generated. By calculating depth maps, the reconstruction proceeds to reconstruct a high-detail, dense 3D point cloud. Special patterns, such as coded markers, can assist photogrammetric software in finding more matching points for alignment. These markers are typically detectable automatically by the software. However, photogrammetric 3D point clouds are initially not scaled or oriented. The use of these markers helps define scale bars and orient the 3D model. In this study, RealityCapture (RealityCapture 2024) was used for photogrammetry, and CloudCompare (Girardeau-Montaut 2022) was utilized for analyzing the 3D point clouds. Calibration was performed using the self-calibration method in RealityCapture, employing the Brown3 Tangential 2 distortion model. According to the previous study, using higher number of markers and scale bars leads to more accurate scaling and high precision photogrammetric 3D models (Torkan et al. 2024).

2.2.2 Sample preparation for photogrammetry

To scale and orient the sample, dual-ring 12-bit markers with predefined distances (Fig. 2 (a)) were used, Pd1 12.376 mm and Pd2 17.5023 mm. These markers were generated using RealityCapture software, and their distances were measured with GIMP software (The GIMP Development Team 2022), providing a resolution of 1 µm. The markers were then printed on sticker paper at a resolution of 1200 DPI. The sample was covered with these coded markers, ensuring that sections covering the fracture outcrops were removed. A platform with a sheet marked by predefined distances was prepared, and the sample was fixed at its center (Fig. 2 (b)). To evaluate the accuracy of the photogrammetry results, four ceramic blocks were strategically placed around the sample in four orientations: horizontally (directions X and Y), vertically, and diagonally (Fig. 2 (b)). The ceramic calibration blocks were 25 mm, 50 mm, 75 mm, and 100 mm, with a resolution of 1 µm.

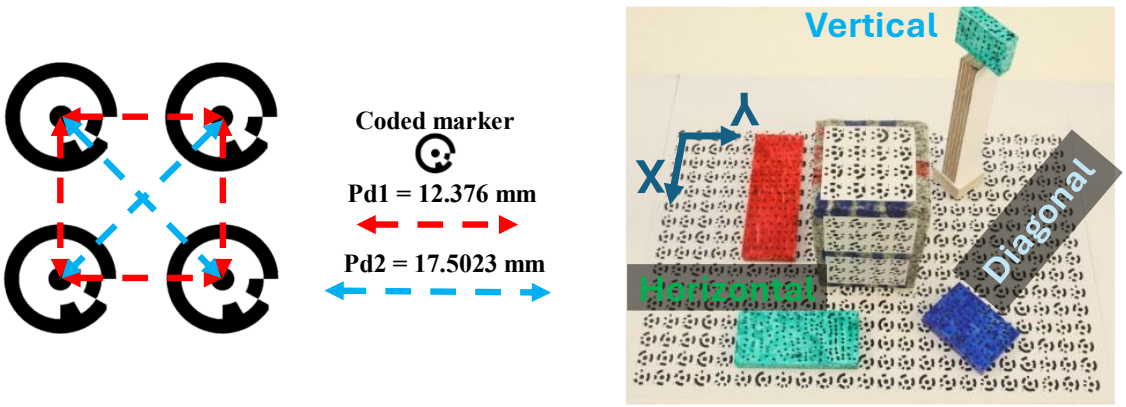

(a) (b)

Fig. 2 (a) Coded markers used for photogrammetry, along with the predefined distances among them; and (b) The sample with a 5 mm dislocation from its initial position in direction X, showing the distribution of the ceramic calibration blocks and the marker sheet. Ceramic calibration blocks were dyed blue, green, and red, with black dots added to enhance their visibility during photography.

2.2.3 Photography

A rotary table was used to capture photos at 9° intervals, resulting in 40 images per full rotation. The illumination was set to 4000 lux. A DSLR Canon camera with a 35 mm lens was positioned at a shooting distance of 50 cm from the sample, achieving a Ground Sample Distance (GSD) of 42 µm, meaning each pixel represented 42 µm in reality. The photogrammetry software further refines accuracy, offering sub-pixel precision that can range from one-fifth to one-twentieth of a pixel. To ensure consistent focus throughout the process, the camera was mounted on a tripod, the lens was manually set to focus at 50 cm, and the focus ring was taped to prevent any accidental adjustments. The camera specifications are detailed in Table 1.

Table 1 Camera specifications

Item	Max resolution [Mpix]	Sensor size [mm × mm]	Image resolution [pix]	Pixel size [µm]	Lens	Lens focal length [mm]	Format of photos	ISO	F-Stop (aperture)
Canon EOS 5DS R DSLR	50.6	36 × 24	8688 × 5792	4.17	Canon EF 35mm f/1.4L II USM	35	JPEG + RAW	100	11

2.2.4 Top and bottom halves of the sample and the well-matched position

To measure the physical aperture, the well-matched sample was photographed as shown in Fig. 3 (a). Photos were captured at four pitch angles: 0°, 30°, 45°, and 60°, with varying focus points. Each half of the sample was scanned separately, using the same pitch angles as in the previous step but with different focal points (Fig. 3 (b)) and using distinct marker sheets for each half (Fig. 2 (b)). Additionally, each half was flipped upside down, and photos were taken at three pitch angles: 0°, 30°, and 60°. It is worth noting that in the upside-down position, the marker sheet was removed.

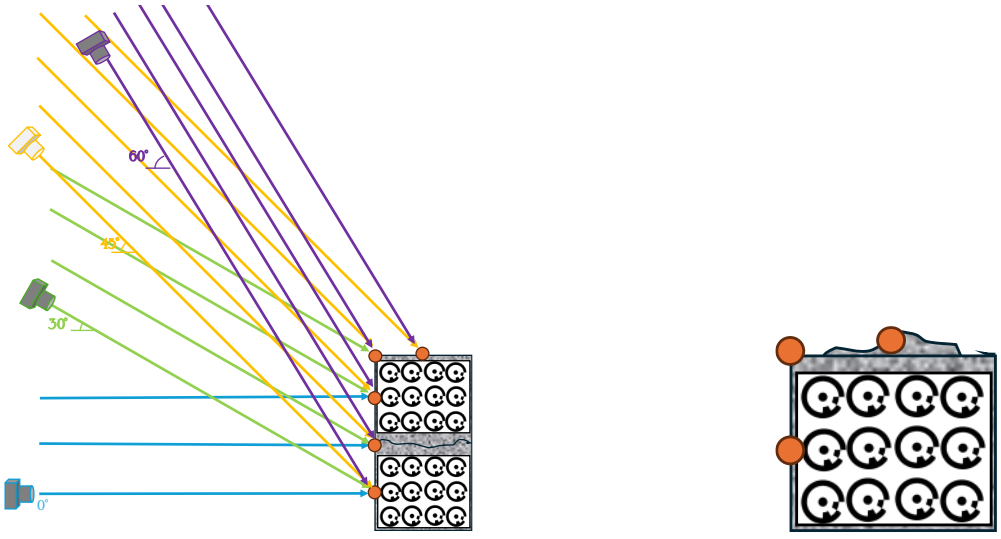

(a) (b)

Fig. 3 Camera positions and pitch angles used for photogrammetry and focal points (a) the well-matched sample and (b) a half.

2.2.5 Reconstructing 3D models

For each photo set, the images were imported into RealityCapture, grouped under the same calibration group, and the coded markers were detected. The photos were then aligned. 3D models of the top and bottom halves were reconstructed with normal detail and then texturized.

For the 3D models of the well-matched positions, three markers located at the bottom-left corner of the bottom half were selected to define a coordinate system (Fig. 4). These markers were reclassified from Tie Points to Ground Control Points (GCPs), enabling the definition of the coordinate system. The selected markers were assigned coordinates as follows: G1 (0, 0, 0), G2 (Pd1, 0, 0), and G3 (0, 0, Pd1). Scale bars were defined using the predefined distances between markers. The 3D model was subsequently realigned to scale and orient it within the defined coordinate system. The coordinates of all markers were extracted as GCPs and imported into the 3D models of both the top and bottom halves to bring them in the same coordinate system.

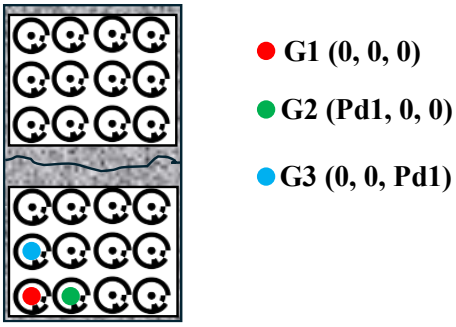

Fig. 4 Defining a local coordinate system for the well-matched sample to extract the coordinate data of other markers.

2.2.6 Non-dislocated physical aperture

After putting the top and bottom halves in the same coordinate system, the 3D models were exported as *.xyz files and imported into CloudCompare. By cropping the exterior body of top and bottom halves and keeping the rough surfaces, by using cloud to cloud distance tool in CloudCompare, the physical aperture in direction Z was calculated.

2.2.7 Dislocated physical aperture

The top half of the sample was displaced in direction X by 1, 2, 3, 4, and 5 mm. These displacements were measured using a caliper with a resolution of 10 µm. The upper surface of the top half was leveled to 0° (horizontally), and non-harmful glue was applied to maintain this position as support. After each displacement, photography and 3D modeling were conducted using the same methods as for the non-dislocated physical aperture. To calculate the physical aperture for the dislocated positions, the rough surfaces that did not overlap were cropped, and measurements were performed only on the overlapped sections (Fig. 5).

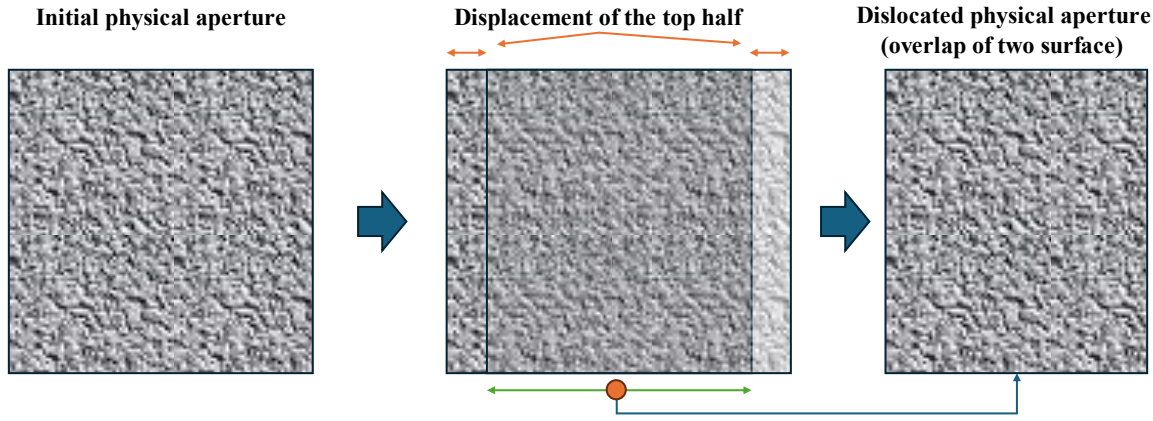

Fig. 5 Calculation of physical aperture after dislocation.

2.3 Accuracy assessment

In this study, two ground truth methods were applied to assess the accuracy of the photogrammetric approach: Root Mean Square Error (RMSE) and ceramic calibration blocks. The RMSE was calculated using Eq. 1, comparing predefined distances with the corresponding digital distances obtained through photogrammetry. After attaching predefined distance markers to the sample, 274 distances were available for scaling and accuracy assessment. The predefined distances were randomly divided into two groups for the photogrammetric 3D model with a 5 mm displacement in direction X. One group was used as scale bars to scale the model, and the other as check bars to assess accuracy. The scale bars were applied first to scale the model, and the check bars were then used to compare the predicted values with the predefined distances. RMSEs were calculated for both scaling and accuracy based on the scale bars and check bars.

$$RMSE = \sqrt{\sum_{i=1}^{n} \frac{(Predefined\ distance_i - Photogrammetric\ distance_i)^2}{n}} \quad (1)$$

Where i refers to the check or scale bar, and n is the total number of predefined distances used for scaling the model.

For the ceramic calibration blocks, after scaling the 3D model, the 3D point clouds of the ceramic blocks were used to measure the distances between two surfaces corresponding to the specified dimensions. These measured distances were then compared with the actual sizes of the ceramic blocks. This comparison helps verify whether the scaling method can accurately scale a 3D model of an object with known dimensions and assess any differences.

3 Result and discussion

3.1 Accuracy assessment

Multiple scale bars were used to assess the accuracy of the photogrammetric 3D models. The scale bars were applied to scale the 3D model, and the check bars were used to evaluate the accuracy of the scaling process. RMSE values were calculated using Equation 1 for the physical aperture with a 5 mm displacement. The RMSE for the scale bars was 36 μm, indicating the deviation between the actual and calculated values by photogrammetry. The RMSE for the check bars was 38 μm, reflecting the difference between the actual and predicted values by photogrammetry. These results demonstrate that the scaling method can accurately scale photogrammetric 3D models. When all predefined distances were used as scale bars to scale the model, the RMSE remained 37 μm, suggesting that increasing the number of scale bars had little impact on the overall accuracy.

For the ceramic calibration blocks, the differences between the actual dimensions and the 3D point cloud measurements for 50 and 75 mm blocks were 16 and 60 μm, further confirming the effectiveness of the scaling method.

3.2 Non- and dislocated physical aperture

After reconstructing the 3D models of the top and bottom halves and calculating the initial (non-dislocated) physical aperture, the physical apertures for displacements of 1, 2, 3, 4, and 5 mm were determined. The variations in physical aperture for these displacements are shown in Fig. 6, illustrating the transition from the initial aperture to the aperture at 5 mm displacement.

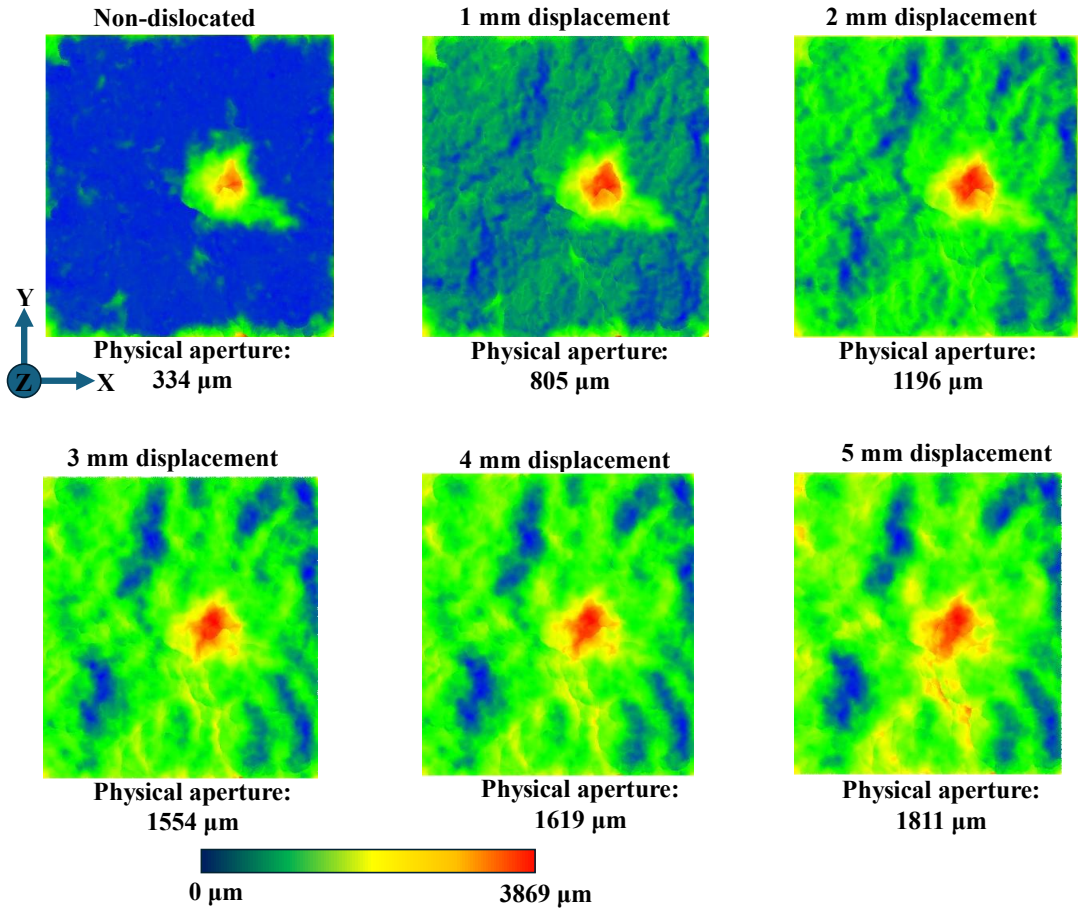

Fig. 6 Physical aperture fields for different dislocations in direction X obtained by 3D photogrammetric models.

The results for physical apertures, obtained using cloud-to-cloud distances in direction Z in CloudCompare, are presented in Fig. 7. As can be seen, with increasing dislocations, the physical aperture also increases. The fitting regression showed a nonlinear trend (quadratic), which can be analyzed as follows: at the beginning of the dislocation stage, the changes in physical aperture are drastic and steep. However, after some displacement, changes begin to change smoother. This behavior could be due to steep asperities playing an important role in changing the physical aperture along the dislocation direction. Once these asperities are surpassed, the changes become less significant. By increasing void spaces through fracture dislocation, the standard deviation of the physical aperture increased. Moreover, the sample size used in this study is too small for more detailed analysis. It is recommended to conduct additional tests with larger sample sizes and further dislocations, for example, conducting to the middle of the samples, for a more comprehensive understanding. If the relationship between displacement and physical aperture is established, it could assist in predicting fluid flow behavior during shear displacement, which requires further investigation.

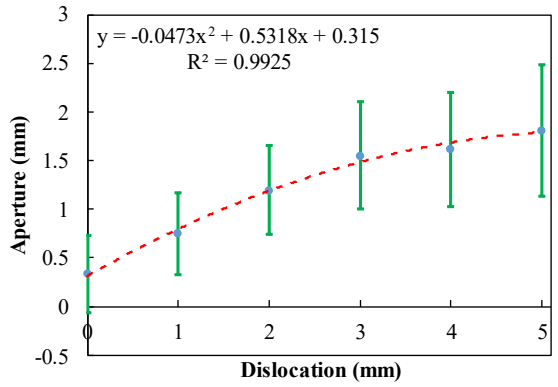

Fig. 7 Physical aperture versus dislocation. The dashed red line shows the fitting trendline and the green lines show the standard deviation of physical apertures for different dislocations.

4 Conclusion

A high-precision photogrammetric method was proposed and evaluated in this study for measuring dislocated physical aperture, which is essential for analyzing shear behavior and fluid flow through fractures. The method was applied to a sample measuring 6 cm × 6 cm × 10 cm, smaller than the typical shear sample sizes (around 10 cm). A large number of predefined distance markers were used as scale bars to measure physical aperture through photogrammetry.

The proposed method enabled the alignment of two separate halves of a sample within the same coordinate system, allowing for the calculation of their relative positions under various configurations. The accuracy was assessed using RMSE by comparing the photogrammetric distances with their actual values and by evaluating ceramic calibration blocks against their photogrammetric 3D models.

Physical aperture was calculated after each dislocation, revealing a nonlinear increasing trend with dislocation, following a quadratic relationship. As dislocation increased and matedness decreased, the physical aperture exhibited consistent growth.

This study demonstrates the ability and feasibility of the photogrammetric method for precisely measuring both non-dislocated and dislocated physical apertures.

Acknowledgment

This work was made possible thanks to the funding provided by the National Nuclear Safety and Waste Management Research Programme SAFER2028, funding numbers SAFER 25/2023 (MIRKA). During the preparation of this work the authors used ChatGPT 4 to check the language and improve the readability. After using ChatGPT, the authors reviewed and edited the content as needed and take full responsibility for the content of the publication.

Author contributions

Conceptualization, M.T.; methodology, M.T.; data collection, S.L.V., M.T.; data analysis, M.T.; writing-original draft preparation, M.T.; visualization, M.T.; writing-review and editing, S.L.V., M.A., L.U., A.A, M.J., M.R.; supervision, M.R.; project administration, M.R. and L.U.; funding acquisition, L.U. All authors have read and agreed to the published version of the manuscript.

References

Barton N (1978) Suggested methods for the quantitative description of discontinuities in rock masses. International Society for Rock Mechanics. International Journal of Rock Mechanics and Mining Sciences & Geomechanics Abstracts 15: 319-368. https://doi.org/10.1016/0148-9062(78)91472-9

Brady BHG, Brown ET (1985) Rock mass structure. Springer, Dordrecht. https://doi.org/10.1007/978-94-011-6501-3_3.

Chen Y, Liang W, Lian H, Yang J, & Nguyen VP (2017) Experimental study on the effect of fracture geometric characteristics on the permeability in deformable rough-walled fractures. International Journal of Rock Mechanics and Mining Sciences 98: 121–140. https://doi.org/10.1016/j.ijrmms.2017.07.003.

Girardeau-Montaut D (2022) CloudCompare V.2.6.1 User Manual. https://www.cloudcompare.org/

Hakami E, Larsson E (1996). Aperture Measurements and Flow Experiments on a Single Natural Fracture. International Journal of Rock Mechanics and Mining Sciences & Geomechanics Abstracts 33 (4): 395-404. https://doi.org/10.1016/0148-9062(95)00070-4.

Hakami E (1995) Aperture distribution of rock fractures. Dissertation at KTH Royal Institute of Technology.

National Research Council (U.S.) (1996) Rock Fractures and Fluid Flow: Contemporary Understanding and Applications. The National Academies Press, Washington DC. https://doi.org/10.17226/2309.

Olsson R, Barton N (2001) An improved model for hydromechanical coupling during shearing of rock joints. International Journal of Rock Mechanics and Mining Sciences 38: 317-329. https://doi.org/10.1016/S1365-1609(00)00079-4.

RealityCapture (2024) RealityCapture 1.5. http://www.capturingreality.com/. accessed in 2024.

The GIMP Development Team (2022) GIMP, V.2.10.32. https://www.gimp.org.

Torkan M, Janiszewski M, Uotinen L, Baghbanan A, Rinne M (2022) Photogrammetric Method to Determine Physical Aperture and Roughness of a Rock Fracture. Sensors 22 (11): 4165. https://doi.org/10.3390/s22114165.

Torkan M, Janiszewski M, Uotinen L, Baghbanan A, Rinne M (2024) High-resolution photogrammetry to measure physical aperture of two separated rock fracture surfaces. Journal of Rock Mechanics and Geotechnical Engineering 16 (8): 2922–2934. https://doi.org/10.1016/j.jrmge.2023.10.003.

Yong R, Wang C, Barton N, Du S (2024) A photogrammetric approach for quantifying the evolution of rock joint void geometry under varying contact states. International Journal of Mining Science and Technology 34 (4): 461–477. https://doi.org/10.1016/j.ijmst.2024.04.001.

Zhang, L. (2005). Engineering Properties of Rocks. Elsevier.

Zimmerman R (2005). Fluid Flow in Rock Fractures proceedings of the Eleventh International Conference on Computer Methods and Advances in Geomechanics, Turin, Italy, 19-24 June 2005.

Zimmerman R, Bodvarsson G (1996) Hydraulic conductivity of rock fractures. Transport in Porous Media23: 1-30. https://doi.org/10.1007/BF00145263.